Ultrahigh-throughput screening enables efficient single-round oxidase remodelling

Journal Article

Author(s):
Debon, Aaron; Pott, Moritz; Obexer, Richard; Green, Anthony P.; Friedrich, Lukas; Griffiths, Andrew D.; Hilvert, Donald

Publication date:
2019-09

Permanent link:
https://doi.org/10.3929/ethz-b-000368514

Originally published in:
Nature Catalysis 2(9), https://doi.org/10.1038/s41929-019-0340-5

ARTICLES
https://doi.org/10.1038/s41929-019-0340-5

nature catalysis

Ultrahigh-throughput screening enables efficient single-round oxidase remodelling

Aaron Debon[1], Moritz Pott[1], Richard Obexer[1], Anthony P. Green[1,4], Lukas Friedrich[2], Andrew D. Griffiths[3] and Donald Hilvert[1*]

Biocatalysis provides a potentially sustainable means of chemical manufacturing. However, the tailoring of enzymes to industrial processes is often laborious and time consuming, which limits the broad implementation of this approach. High-throughput screening methods can expedite the search for suitable catalysts, but are often constrained by the need for labelled substrates. The generalization of such techniques would therefore significantly expand their impact. Here we have established a versatile ultrahigh-throughput microfluidic assay that enables isolation of functional oxidases from libraries that contain up to 10^7 members. The increased throughput over prevalent methods led to complete active-site remodelling of cyclohexylamine oxidase in one round of directed evolution. A 960-fold increase in catalytic efficiency afforded an enzyme with wild-type levels of activity for a non-natural substrate, allowing biocatalytic synthesis of a sterically demanding pharmaceutical intermediate with complete stereocontrol. The coupled enzyme assay is label free and can be easily adapted to re-engineer any oxidase.

Chiral amines play an indispensable role in the production of high-value chemicals. Approximately 40% of active pharmaceutical ingredients (APIs) depend on optically active amines as intermediates during production[1], and consequently asymmetric amine synthesis has been identified as one of the key challenges towards a greener and more sustainable chemical industry[2]. In recent years, biocatalysis has emerged as an attractive and competitive technology for chiral amine synthesis[3–6], as enzymes display high levels of activity and stereocontrol, function under ambient conditions and can, in principle, be readily adapted for industrial purposes using laboratory evolution. Indeed, engineered enzymes are applied in the large-scale manufacture of APIs and key chiral pharmaceutical building blocks[7,8]. Adopting these biocatalysts has decreased the number of synthetic steps required, circumvented the need for costly transition metal catalysts, reduced the demand for organic solvents and delivered products with increased (optical) purity, thus alleviating the need for expensive downstream purification steps.

Amine oxidases have proved to be especially effective for the production of optically pure amines through deracemization, a process that combines oxidation catalysed by an enantioselective enzyme and a non-selective chemical reducing agent[9]. Cycles of selective oxidation and non-selective reduction lead to the accumulation of a single enantiomer in high yield. For example, monoamine oxidase from *Aspergillus niger* and cyclohexylamine oxidase from *Brevibacterium oxydans* (CHAO) have been engineered to deracemize chiral auxiliaries[9] as well as secondary[10] and tertiary[11] amine-containing APIs and pharmaceutical building blocks[12]. Engineered amine oxidases have also been exploited in oxidative desymmetrization processes, most notably in the large-scale synthesis of a key chiral pyrrolidine derivative used in the production of the hepatitis C virus protease inhibitor boceprevir[8].

Despite these signal successes, adapting oxidases to perform new tasks remains a challenging, labor intensive endeavour that restricts the potential impact of biocatalysis on many industrial processes. Although powerful, directed evolution experiments are generally time consuming (months to years) and costly (in man hours, consumables and equipment)[13], rendering them incompatible with the fast pace of business and preventing broader implementation of enzymes in chemical synthesis[14]. To increase the viability of biocatalysis for green chemistry, methods that accelerate directed evolution are urgently needed[15–18].

Amine oxidases can be assayed by coupling the universal hydrogen peroxide by-product formed during cofactor recycling to a reaction that generates a dye (Fig. 1a), providing a versatile method of screening in microtitre plates[19], on agar plates[9] and in cells[20]. Nevertheless, engineering the monoamine oxidase from *A. niger* for the boceprevir manufacturing process required introduction of 65 mutations. Even with dedicated infrastructure for automated and high-throughput enzyme engineering, biocatalyst optimization was arduous with most rounds contributing only single-digit improvements in activity.

Enzymatic assays using monodisperse emulsions generated on microfluidics chips have emerged as a powerful ultrahigh-throughput method in the search for novel biocatalysts[17]. This approach utilizes picolitre to nanolitre-volume aqueous droplets, stabilized by surfactant, in an inert, fluorinated oil as independent microreactors that contain single cells (Fig. 1b)[21]. On-chip microfluidic modules allow multiple operations, which include droplet production, splitting, fusion, reagent addition, incubation, fluorescence detection and fluorescence-activated droplet sorting (FADS), all at kilohertz frequencies[22,23]. To screen for novel enzymes, single cells that express individual variants are typically encapsulated in droplets containing a fluorogenic substrate. Active enzymes can be displayed on the cell surface[13], secreted[24,25] or released by cell lysis[26]. Compartmentalization thus links genotype and the fluorescent product, enabling the enrichment of rare, but active, variants from large libraries by sorting according to activity (Fig. 1c). FADS increases screening power dramatically compared to low- or medium-throughput microtitre plate-based techniques.

[1]Laboratory of Organic Chemistry, ETH Zurich, Zurich, Switzerland. [2]Institute of Pharmaceutical Sciences, ETH Zurich, Zurich, Switzerland. [3]Laboratory of Biochemistry, École Supérieure de Physique et de Chimie Industrielles de la Ville de Paris (ESPCI Paris), CNRS UMR 8231, PSL Université, Paris, France. [4]Present address: Manchester Institute of Biotechnology, School of Chemistry, University of Manchester, Manchester, UK. *e-mail: hilvert@org.chem.ethz.ch

Approximately 10^7 variants can be assayed per experiment in a sensitive manner, reducing the expenditure of time and cost in consumables by several orders of magnitude[13].

Here we describe a label-free, ultrahigh-throughput, FADS-based coupled assay for oxidase engineering and its application to rapid remodelling of the CHAO active site for an industrially relevant substrate for which the original enzyme showed only low activity. We were able to generate an enzyme with a three orders of magnitude increase in catalytic efficiency and wild-type levels of activity on the non-natural substrate in a single round of directed evolution.

Results

FADS of cyclohexylamine oxidase. Although CHAO oxidizes a range of primary (*S*)-configured amines, it is reportedly inactive with 1-phenyl-1,2,3,4-tetrahydroisoquinoline (PheTIQ (**7**))[27], whose (*S*)-enantiomer is a key precursor of the blockbuster drug solifenacin. Kinetic characterization of the wild-type enzyme using a high catalyst concentration revealed that it shows no detectable activity on the (*S*)-enantiomer but possesses a k_{cat}/K_M of $10 \pm 1\,M^{-1}\,s^{-1}$ for the (*R*)-enantiomer, which is three orders of magnitude lower than the value reported for the native cyclohexylamine substrate[28].

To remodel the active site of CHAO to accept PheTIQ, we targeted eight residues for mutagenesis: 7 of the 11 residues that are within 5.5 Å of the bound cyclohexanone in the crystal structure of wild-type CHAO (Tyr321, Phe368, Pro422, Thr198, Leu199, Phe351 and Leu353) plus Met226, which is located a little farther away in the substrate diffusion channel (Supplementary Fig. 1). With the exception of Phe351 and Pro422, which are absolutely conserved, phylogenetic analysis shows that most of these residues have been subjected to conservative mutation in natural CHAO homologues (Supplementary Table 1). All eight residues were randomized simultaneously using primers with either DYT codons, which encode six amino acids (A, S, T, V, I and F), or the BYT codon for Pro422, which encodes A, S, P, V, L and F. The codons were designed to incorporate hydrophobic side chains in a range of sizes and alcohols for hydrogen-bonding interactions with the substrate, thus maintaining the overall polarity of the native binding pocket but allowing variation in shape. The resulting library contained 1.7×10^6 theoretical members, with no diversity lost to stop codons and, as each amino acid is specified by a single codon, no frequency bias for one amino acid over another (Supplementary Table 2).

The gene library was expressed in *Escherichia coli* and the cells were injected into a microfluidic chip, where they were mixed with lysis agents, *rac*-PheTIQ and a reporter cascade that consisted of horseradish peroxidase (HRP) and the fluorogenic dye Amplex UltraRed, and compartmentalized in 15 pl droplets with, on average, 0.3 cells per droplet to ensure that few droplets (<4%) contained more than one cell. To exert evolutionary pressure on k_{cat}, screening was performed at a substrate concentration higher than the Michaelis constant for wild-type CHAO (4 mM versus ~1 mM (Supplementary Table 4)). The library was sorted three times, collecting the 0.1% most active droplets in each population. The starting population consisted of $>10^7$ transformants, which represents a greater than threefold oversampling of all the possible variants. After sorting, plasmid DNA was purified from the collected droplets. The genes were amplified by PCR, subcloned and transformed back into *E. coli* cells. The resulting transformants were used for the next sort. In the first two sorts, the emulsion was incubated for 2 h off-chip prior to screening. For the final sort, the emulsion was only incubated for 15 min on-chip to increase screening stringency. The purified plasmids from this sort were used directly to transform *E. coli* for further analysis of the enriched population.

Individual variants from each cycle were analysed and compared to the starting point using a colorimetric lysate-based activity assay in microtitre plates. The fraction of clones with an improved activity increased from 3% before sorting to 43% after the third round of sorting, and the mean activity of the sorted population increased 78-fold compared to the unsorted library. The most active clones were chosen for sequencing (Supplementary Fig. 2 and Supplementary Table 3). Remarkably, the entire workflow, which included library creation, three rounds of FADS, a microtitre plate assay, isolation and sequencing of hits, was performed in under two weeks (Supplementary Fig. 3).

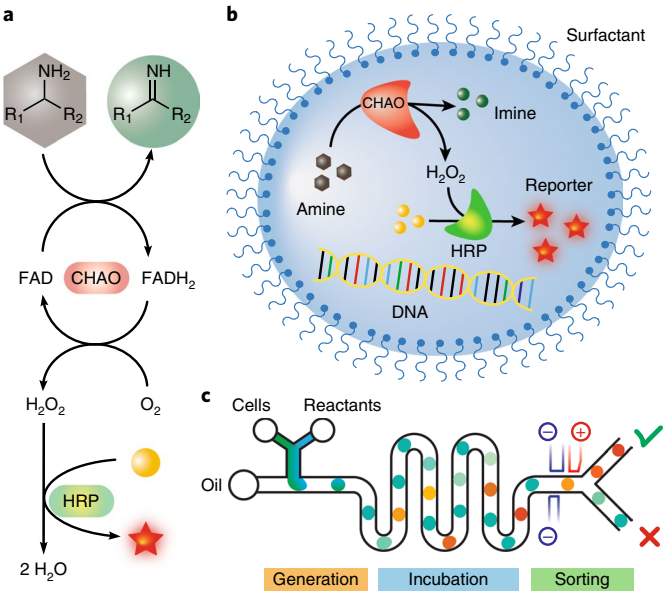

Fig. 1 | Detection strategy and FADS of CHAO. a, CHAO converts amines into the corresponding imine, reducing 1 equiv. of flavin adenine dinucleotide (FAD). Oxygen-dependent cofactor recycling produces equimolar amounts of hydrogen peroxide, which is detected by the downstream oxidation of a fluorogenic substrate by HRP. **b**, Surfactant stabilized droplets act as a diffusion barrier for catalyst-encoding DNA and the fluorescent reporter generated in the coupled enzymatic reactions catalysed by CHAO and HRP. **c**, Schematic representation of a typical microfluidic chip[29]. Single cells are co-encapsulated with lysis agents, substrate and the detection cascade in droplets dispersed in fluorinated oil. The cells are lysed in the droplets, which releases the enzyme and, after incubation, the droplet fluorescence is analysed. Droplets with fluorescence that exceeds a defined threshold are sorted via dielectrophoresis and collected. The DNA of the active clones is pooled, recovered by PCR and subcloned for the next round of sorting and analysis.

Isolation and characterization of PT.1. The three most active clones from the third sort had identical amino acid sequences, differing only in silent mutations that arose spontaneously during PCR, which indicates that they originated from independent sorting events. This variant, referred to as PT.1, has five amino acid changes compared to wild-type CHAO: L199V, M226T, Y321S, L353I and P422S (Fig. 2a and Supplementary Fig. 4). PT.1 was purified and kinetically characterized with both enantiomers of PheTIQ (Supplementary Fig. 5). It has a k_{cat}/K_M of $9{,}400\,M^{-1}\,s^{-1}$ with (*R*)-PheTIQ, which constitutes a 960-fold improvement compared to wild-type CHAO with the same substrate (Fig. 2b) and is similar to the reported catalytic efficiency of the wild-type enzyme with its native substrate cyclohexylamine ($k_{cat}/K_M = 10{,}630\,M^{-1}\,s^{-1}$) (ref. [28]). The improvement is mainly due to a 340-fold larger turnover number ($k_{cat} = 3.2\,s^{-1}$ versus $0.0095\,s^{-1}$). Furthermore, PT.1 is highly stereoselective for the (*R*)-enantiomer, with a specificity constant $S = (k_{cat}/K_M)_R/(k_{cat}/K_M)_S = 4{,}200$ (Supplementary Table 4).

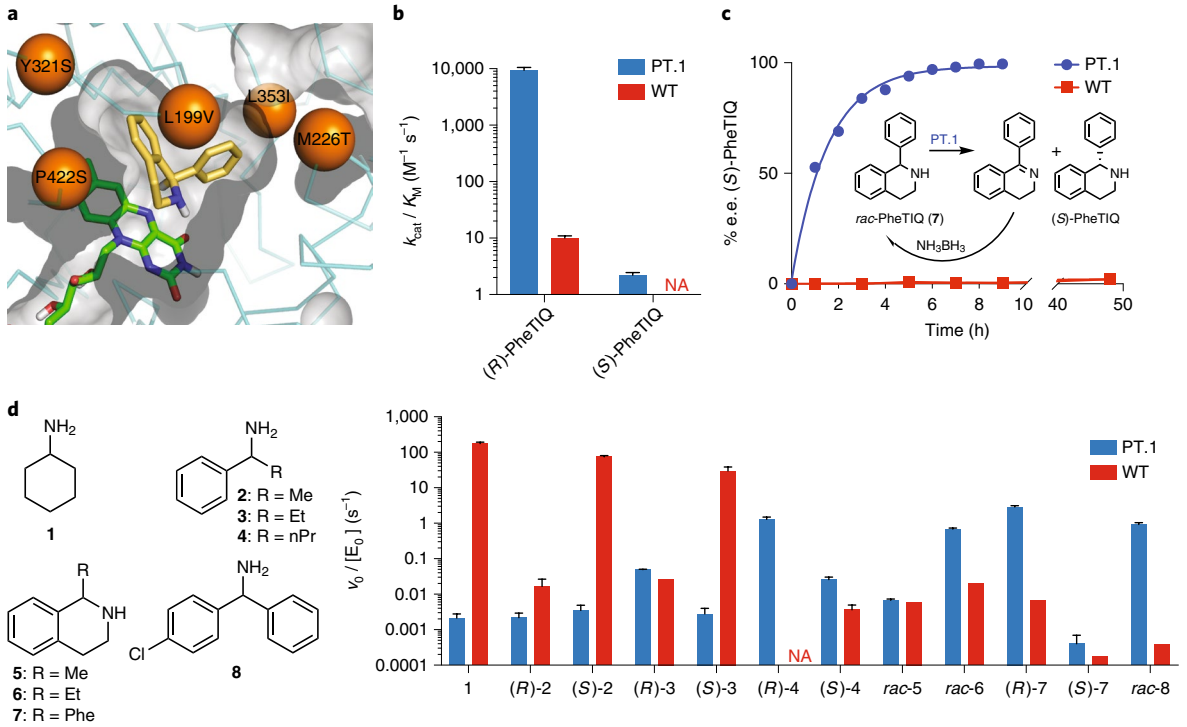

Fig. 2 | Characterization of the engineered PT.1 variant and wild-type CHAO. a, Active site model of PT.1 with the FAD cofactor in green, (*R*)-PheTIQ in yellow and the five mutated amino acids in orange. **b**, The catalytic efficiency of PT.1 towards (*R*)-PheTIQ is improved by almost three orders of magnitude compared to the wild-type enzyme. Furthermore, PT.1 displays an impressive specificity constant (*S*) of 4,200. **c**, The isolated variant, PT.1, was used to deracemize PheTIQ in combination with ammonia borane. Deracemizations mediated by PT.1 resulted in the accumulation of (*S*)-PheTIQ (>99% e.e.) over the course of several hours, whereas analogous reactions with wild-type CHAO gave no enrichment in optical purity. **d**, Comparison of the substrate scope of PT.1 and wild-type CHAO. The initial reaction velocities with 2 mM substrates **1**–**8** and nano- to micromolar enzyme concentrations were determined by monitoring the coupled reaction between the hydrogen peroxide by-product, 4-aminoantipyrine, and vanillic acid catalysed by HRP at 498 nm. The evolved variant preferentially oxidized bulky amines **6**–**8**, whereas wild-type CHAO preferred smaller primary amines such as the native substrate **1** and α-benzyl amines **2** and **3**. Interestingly, with larger α-substituents, as in **3** and **4**, PT.1 exhibited a switched stereospecificity compared to wild-type. All error bars indicate the s.d. of three measurements using independent batches of purified enzyme; NA, not active.

Analysis of the substrate scope of PT.1 revealed a dramatic change in substrate acceptance (Fig. 2d). Whereas the wild-type enzyme prefers primary amines, such as cyclohexylamine and the (*S*)-configured α-benzyl amines **2** and **3**, PT.1 is almost inactive towards these substrates. Instead, it converts (*R*)-configured α-benzyl amines with sterically demanding minor substituents (for example, **4** and **8**) and bulky secondary amines like **6** and **7**.

Biocatalytic transformations. Purified PT.1 and wild-type CHAO were compared for their efficacy in producing the optically pure (*S*)-PheTIQ solifenacin precursor by deracemization of (*rac*)-PheTIQ (**7**, Fig. 2c). The processes were initiated by adding purified oxidase to a buffered solution of the racemic substrate and 4 equiv. of ammonia borane complex as the reducing agent. Once the optical purity converged, the product was extracted using organic solvent. At a 0.05% catalyst loading, PT.1 achieved a 99% e.e. for the desired (*S*)-enantiomer within nine hours, whereas the wild-type enzyme did not enrich either enantiomer over two days under the same conditions (Fig. 2c and Supplementary Fig. 6d).

Analogous results were obtained when the reaction with (*rac*)-**7** was carried out with whole cells that produced the PT.1 variant. The latter conditions were therefore used in deracemization experiments with the other tetrahydroisoquinoline derivatives shown in Fig. 2 (Table 1). Compound **6**, which has an ethyl rather than a phenyl substituent, afforded (*S*)-EthylTIQ with an e.e. of 98% after 36 hours. In contrast, little enantiomeric enrichment (e.e. 5%) was observed for compound **5** with the even smaller methyl substituent, which reflects both its modest steric demands and substantially lower activity with the enzyme.

Attempts to deracemize primary amines such as **3**, **4** and **8** were complicated by the competitive hydrolysis of the iminium ion product of the enzymatic reaction before it could be reduced by the ammonium borane, which leads to the accumulation of unwanted ketone and/or alcohol side products. Nevertheless, compound **4**, which has a phenyl group and a propyl group that are readily distinguishable and sufficiently large to bind productively to the enlarged PT.1 pocket, gave (*S*)-1-phenylbutylamine in 35% yield and 50% e.e. after 48 hours of reaction. In contrast, no enantiomeric enrichment was observed for **3** or **8**. Although kinetic measurements with the individual enantiomers of **3** indicate an *S* value of 17 (Fig. 2d), this compound is a relatively poor substrate for the enzyme, which makes preparative deracemization impractical over a reasonable time frame. Although **8** is a good substrate for the enzyme, the remodelled PT.1 binding pocket is apparently unable to distinguish between the phenyl and *p*-chlorophenyl substituents.

Molecular modelling. To gain insight into the molecular basis of the switch in substrate specificity, we preformed docking experiments on wild-type CHAO (PDB ID 4i59) and an in silico model of the optimized PT.1 catalyst with both (*R*)- and (*S*)-PheTIQ. Although the starting enzyme cannot accommodate either substrate enantiomer without substantial steric clashes, the active site

Table 1 | Preparative deracemization reactions

Entry	Compound	e.e. (%)	Yield (%)	Time (h)
1	**3**	0	ND	48
2	**4**	50 (*S*)	35	48
3	**5**	5 (*S*)	75	36
4	**6**	98 (*S*)	81	36
5	**7**	99 (*S*)	71	9
6	**8**	0	ND	48

For compound **7**, deracemization was carried out with 5 μM purified enzyme and 4 equiv. NH_3BH_3 in 1 M sodium phosphate buffer at pH 7.0 at 30 °C. For the other substrates, the reactions were performed with whole cells that produced PT.1 (Methods). The e.e. values were determined by HPLC with a chiral stationary phase. ND, not determined.

substitutions remodelled the binding pocket for shape complementary recognition of the larger PheTIQ substrate. In particular, the Y321S and P422S mutations carved out additional space for the tetrahydroisoquinoline ring, which allowed the experimentally preferred (*R*)-PheTIQ to dock in a catalytically competent orientation proximal to the flavin cofactor (Supplementary Fig. 7a). Although (*S*)-PheTIQ also fits in the enlarged pocket, it adopts an orientation that precludes hydride transfer to the cofactor because the relevant C–H bond points away. A hydrogen-bonding interaction between the (*S*)-PheTIQ amine and the side chain of Ser422, which was introduced during optimization, and the backbone carbonyl of Thr198 favours this unproductive pose (Supplementary Fig. 7b). Mutation of Met226 in the substrate diffusion channel to threonine matches previous reports that show that smaller residues at this site boost activity for a multitude of substrates[28], probably owing to the improved substrate uptake and/or product release.

Discussion

Enzymes have the potential to play a major role in reducing the environmental impact of chemical manufacture. The dramatically enhanced screening power of droplet microfluidics compared to microtitre plate-based techniques can facilitate both their discovery and optimization. Screening large libraries from bacteria[23,26,29], yeast[13,25] and filamentous fungi[24] and large (>1 million genes) metagenomic libraries that comprise environmental DNA from microorganisms[30] has yielded active hydrolases[30,31], peroxidases[13], cellulases[32] and aldolases[29]. Screening pairs of enantiomeric substrates with different coloured fluorescent leaving groups even enables the discovery of enantioselective catalysts[31]. Non-fluorescent screening of enzymatic reactions in droplets using absorbance-activated droplet sorting and Raman-activated droplet sorting promises to expand these capabilities even further[33,34].

If biocatalysis is to be competitive with conventional synthesis, it has been suggested that directed evolution efforts to adapt natural and designed enzymes for specific tasks need to become at least an order of magnitude faster[14]. Droplet microfluidics is poised to make this goal a reality. It has already proven efficacious in cases in which directed evolution using microtitre plate-based approaches fail because an apparent local fitness plateau has been reached, from which it is only possible to escape by screening a larger number of variants. For instance, the directed evolution of an artificial aldolase using droplet microfluidics enabled the best enzyme from a stalled microtitre plate screen to be improved 30-fold to give a $>10^9$ rate enhancement that rivals the efficiency of natural class I aldolases[29].

Nevertheless, most examples of enzyme evolution using droplet microfluidics to date have focused on improving enzymes that already show important levels of activity over multiple rounds of evolution and use fluorogenic model substrates of little industrial interest. As highlighted here, coupled enzyme assays have the potential to generalize this approach. The implementation of a simple means to link hydrogen peroxide formation with a fluorescent readout enabled a time-efficient isolation of active amine oxidases from large libraries (here 1.7×10^6 permutations of eight residues) by FADS. In a single round of evolution, a nearly three orders of magnitude leap in catalytic efficiency and a radically reshaped substrate profile was achieved. This approach outperformed the conventional evolutionary optimization of monoamine oxidase from *A. niger* for PheTIQ, which entailed separate screenings of six different libraries and a second round of mutagenesis to produce a catalyst with a k_{cat}/K_M an order of magnitude lower than PT.1[35], underscoring the advantage of simultaneously mutating multiple residues to facilitate the discovery of novel active site configurations.

In conclusion, our work highlights FADS as a powerful and versatile technology for rapidly engineering oxidases to perform new and valuable functions. It enables the engineering of a tailor-made, synthetically useful enzyme for an important chiral API precursor in a timeframe compatible with today's product plant development. FADS has the flexibility of a typical microtitre plate assay, which makes it easy to adapt established screening approaches. In contrast to in cellulo assays[20], it is not limited by poor uptake of substrates or product diffusion. Moreover, the coupled assay used here is label free, obviating the need for surrogate substrates through detection of a common by-product, and should be readily transferrable to any other oxidase. These capabilities promise to facilitate a rapid tailoring of substrate specificity for a whole class of industrially important enzymes for the production of chiral amines, secondary thiols[36] and alcohols[37]. This approach should be easily extendable to other enzyme families that produce detectable (by-)products during catalytic turnover.

Methods

Materials. Chemicals were purchased from Sigma, ABCR, Acros, Fluorochem, Thermo Fisher Scientific and Dow Corning. Chemical standards for (*R*)- and (*S*)-1-phenyl-1,2,3,4-tetrahydroisoquinoline (*R*-**7** and *S*-**7**) were bought from Toronto Research Chemicals and TCI Chemicals, respectively. Compounds (*R*)-**7** and (*S*)-**7** were further purified by recrystallizing the HCl salt in ethanol and diethyl ether, filtering and drying in vacuo. Amplex UltraRed was purchased from Thermo Fisher Scientific.

General methods. NMR spectra were recorded on an AVIII 400 (^{1}H 400 MHz, ^{13}C 100 MHz) spectrometer. Small molecules were further analysed by liquid chromatography–mass spectroscopy (Waters H-class UPLC/SQD-2) using an Acquity UPLC BEH C-18 column (50 × 2.1 mm, 1.7 μM), 1 μl injection, monitoring ESI+, solvent A = H_2O + 0.1% trifluoroacetic acid, solvent B = MeCN + 0.1% trifluoroacetic acid, flow-rate = 1 ml min^{-1}, initial conditions = 5% B, 0–1.5 min ramp to 80% B, 1.5–2 min ramp to 100% B, 2–2.2 min = 100% B, 2.2–2.3 min ramp to 5% B, 2.3–3 min re-equilibration = 5% B.

Construction of pKTNTET-CHAO_Kan. The plasmid pACYC-6His-CHAO[38] was used to amplify the wild-type CHAO gene with primers *chao* fw and *chao* rv (Supplementary Table 5), which also introduced 5′ NdeI and 3′ SpeI restriction sites. The insert was purified by agarose gel electrophoresis. The gene and the plasmid pKTNTET-0[39] were both digested with NdeI and SpeI-HF (New England Biolabs) overnight at 37 °C and purified by agarose gel electrophoresis. The fragments were ligated using T4 DNA ligase (New England Biolabs) overnight at 16 °C and purified using Clean and Concentrator 5 Kit (Zymo Research). The resulting construct, pKTNTET-6His-CHAO_Amp, was transformed into XL10-Gold (Agilent) by electroporation. pKTNTET-6His-CHAO_Amp and pET-29b(+) (Novagen) were digested with BspHI, excising their respective antibiotic resistance markers, and the relevant fragments were purified by agarose gel electrophoresis. The kanamycin resistance cassette of pET-29b(+) was ligated into the pKTNTET-6His-CHAO vector for 1 h at room temperature, and the resulting construct was used to transform XL1-Blue cells plated on selective medium. The resulting pKTNTET-6His-CHAO_Kan plasmid was verified by sequencing (Microsynth).

Library generation. Cloning primers and primers for cassette mutagenesis were purchased from Microsynth AG. Six pairs of primers were designed to introduce one BYT and seven DYT degenerate codons into the wild-type gene

(Supplementary Table 6). Seven fragments were generated in individual PCR reactions, purified by agarose gel electrophoresis and assembled by overlap extension PCR[40]. The resulting full-length library amplicon and pKTNTET-6His-CHAO_Kan plasmid were digested with NdeI and SpeI-HF endonucleases overnight at 37 °C. The digested gene fragment was purified using Clean and Concentrator 5 Kit, whereas the plasmid was purified by agarose gel electrophoresis and further desalted using Clean and Concentrator 5 Kit (Zymo Research). The fragments were ligated with T4 DNA ligase at 16 °C overnight and desalted prior to electroporation into XL1-Blue cells.

Microfluidic set-up. The optical device used in this study is described by Obexer et al.[29]. In brief, the set-up consisted of a laser combiner (Omicron Laserage GmbH) for illumination with a 375 nm diode laser and a 561 nm SPPS laser. An inverted fluorescence microscope was used to detect fluorescence using photomultipliers (H10722-30, Hamamatsu Photonics) and corresponding single bandpass filters, FF01-488/561/635 and FF01-609/57-25 (Semrock), for detection at 448 and 609 nm, respectively. A high voltage amplifier (632B, Trek) was used to induce the dielectrophoretic sorting pulses. The photomultiplier tubes and high voltage controller were connected to a field-programmable gate array card (NI USB-7856R R Series Multifunction RIO with Kintex-7 160T FPGA (National Instruments)) and connected to a computer that required a run time engine (National Instruments). The gain of the photomultiplier tubes and the high voltage amplifier were controlled and the signals recorded using custom-made LabView software.

Microfluidic chip production. The design of the chips used and the production of the photomasks are described elsewhere[29,41]. A droplet maker with two aqueous inlets and an oil inlet was used to collect droplets off-chip. These emulsions were sorted on a separate device with two inlets for emulsions, two inlets for spacing oil, and two outlets. For on-chip incubation a 15 min delay line, designed to keep an equal time distribution of the droplets[42], connected a T-junction droplet maker with three aqueous inlets and one oil inlet with a sorting device. A Sylgard 184 base and curing agent (Dow Corning) were mixed in a 10:1 ratio and cast into silicon-SU8 moulds (Wunderlichips). A desiccator was used to remove bubbles from the liquid polydimethylsiloxane (PDMS). The degassed chips were cured at 90 °C for 30 min. The resulting PDMS slab was separated from the mould. Inlets, outlets and connections for the electrodes were punched using surgical punchers (Shoney Scientific) with a 0.3 mm diameter. The PDMS slabs and glass slides (Corning) were cleaned using water and isopropanol and dried at 90 °C. The PDMS slabs and glass slides were bonded together using a plasma cleaner (PDC-32G, Harrick Plasma) at 0.5 mbar for 30 s and incubated at 90 °C overnight. Chips that contained electrodes were placed on a hotplate heated to 90 °C, a InBiSn (51:32.5:16.5) alloy (Indium Corporation of America) was melted into the electrode channels, and copper cables were inserted into the inlets[43]. The finished chips were treated with trichloro(1H,1H,2H,2H-perfluorooctyl)silane (Sigma Aldrich) in vacuo overnight.

Microfluidic assay. The library was transformed by electroporation into XL1-Blue *E. coli* cells and recovered in 50 ml of Super Optimal broth with Catabolite repression (SOC) at 37 °C with shaking at 230 r.p.m. for 1 h before adding kanamycin to a concentration of 25 μg ml^{-1}. After 3 h, 15 ml of culture were used to inoculate a 50 ml LB culture (25 μg ml of kanamycin), which was grown at 37 °C with shaking at 230 r.p.m. After reaching an OD_{600} of 0.3 the temperature was lowered to 20 °C and gene expression induced by supplementing tetracycline to a final concentration of 2 μg ml^{-1}. After overnight expression, 2 ml of the expression culture were harvested by centrifugation at 3,500*g* and 4 °C and were washed three times with 1 ml of supplemented M9 medium (47.6 mM Na_2HPO_4, 22 mM KH_2PO_4, 8.5 mM NaCl, 18.6 mM NH_4Cl, 0.1 mM $CaCl_2$, 1 mM $MgSO_4$, 0.4% glucose, 5 μg ml^{-1} thiamine, 0.08% yeast ForMedium Complete Supplement Mixture (ForMedium), 1× US* trace element mix[44], pH 7.5). Cells were resuspended, filtered through a 5 μm syringe filter (Millipore), supplemented with 30% Percoll (equilibrated with 10× M9 salts) and 2 U ml^{-1} DNAse I (New England Biolabs) and diluted to an OD_{600} of 0.04 or 0.06 for off-chip storage or on-chip storage, respectively.

Off-chip storage. The emulsion was generated with a flow focusing nozzle[45] at a 300 μl h^{-1} flow for the oil phase (Novec HFE-7500 fluorinated oil (3 M) that contained 2% (w/w) 008-FluoroSurfactant (RAN Biotechnologies)) and 100 μl h^{-1} flow for the two aqueous phases, which generated 15 pl droplets at a frequency of 3 kHz. The cell suspension was co-encapsulated with a solution that contained 4 U HRP, 11 μM esculin, 2 mg ml^{-1} lysozyme, 4 mg ml^{-1} polymyxin B, 0.4 wt% Pluronic F127, 0.4 mM Amplex UltraRed, 10 μM EGTA, 20 μM EDTA, 8 mM substrate and 4% dimethylsulfoxide (DMSO) in 50 mM sodium phosphate buffer at pH 7.0. The emulsion, which contains an average of 0.3 cells per droplet, was collected in a 1 ml syringe purged with HFE-7500. After an incubation of approximately 2 h at room temperature, droplets were reinjected into the sorting device at a flowrate of 40 μl h^{-1} and spaced by injecting Novec HFE 7100 oil (3 M) at a flow-rate of 650–750 μl h^{-1}. The emulsion was sorted with an electric pulse frequency of 15 kHz, a voltage of 620 kV and a pulse length that ranged from 0.5 to 0.8 ms. The droplets were sorted at a frequency of ~1,000 Hz.

On-chip incubation. Droplets were generated at a T-junction[46] with the oil phase (Novec HFE-7500 fluorinated oil (3 M) that contained 2% (w/w) 008-FluoroSurfactant (RAN Biotechnologies)) flowing at 30 μl h^{-1} and all three aqueous phases at 20 μl h^{-1}. A lysis mixture that contained 6 U HRP, 15 μM esculin, 3 mg ml^{-1} lysozyme, 6 mg ml^{-1} polymyxin B, 0.6 wt% Pluronic F127, 15 μM EGTA and 30 μM EDTA in 50 mM sodium phosphate buffer pH 7.0 was injected alongside the cell suspension and a separate detection and substrate mixture that contained 0.6 mM Amplex UltraRed, 3 μM esculin, 12 mM substrate and 3% (v/v) DMSO in 50 mM sodium phosphate buffer at pH 7.0. The emulsion, which contained an average of 0.3 cells per droplet, was spaced with Novec HFE-7100 oil (3 M) at a flow-rate of 650–750 μl h^{-1}. Sorting parameters were identical to those described above.

Generally, droplet size was determined using the fluorescence of esculin excited at 375 nm and measured at 448 nm. CHAO activity is proportional to the fluorescence, excited at 561 nm and detected at 609 nm, which results from the HRP-catalysed oxidation of Amplex UltraRed through hydrogen peroxide. Although the total number of active droplets is unknown at the outset of a sorting experiment, the distribution of measured activities usually converges within seconds and changes only slowly over time. Based on the initial distribution, the sorting gate was set to collect the top 0.1% of droplets that displayed the highest fluorescence. For off-chip incubations, the active population shifts over time, which requires periodic adjustment of the threshold, whereas incubation times are uniform for on-chip incubation, so readjusting the sorting gate is seldom necessary. Although complete coverage of a library is not a necessity for a successful directed evolution, the chances of seeing every variant of the 10^6 library members should be ~99%, according to Bosley and Ostermeier[47], assuming an occupancy of 22% singly encapsulated cells, an average sorting frequency of 1 kHz, and ~9 h sorting runs. The sorted emulsion was broken by adding 75 μl of 1H,1H,2H,2H-perfluorooctanol and 15 μl of 10 mM Tris-HCl (pH 8), 10 mM EDTA, 100 mM NaCl, 1% Triton X-100 and 1 mg ml^{-1} proteinase K. After 1 h of incubation at room temperature, DNA was recovered using the DNA Clean and Concentrator 5 Kit and amplified by PCR using JumpStart Taq DNA Polymerase (Sigma Aldrich) (30 s 94 °C, 34 × (30 s 94 °C, 30 s 55 °C, 2 min 72 °C), 10 min 72 °C and final hold at 4 °C) using *chao* fwd and *chao* rv primers. The PCR product was purified by agarose gel electrophoresis and subcloned into the pKTNTET_Kan vector and used to transform electrocompetent XL1-Blue cells. After the third round of sorting the extracted plasmids were directly used to transform electrocompetent XL1-Blue cells. Single clones from each round were further analysed in a microtitre plate assay.

Microtitre plate assay. After each round of microfluidic sorting, the subcloned library or extracted plasmids was transformed by electroporation into XL1-Blue cells and plated on LB agar that contained 25 μg ml^{-1} kanamycin. Single colonies from the transformations alongside three wild-type control colonies were used to inoculate precultures on a microtitre plate that contained 150 μl of LB medium, supplemented with 25 μg ml^{-1} kanamycin and the plates were sealed with a gas-permeable membrane (Breathe Easy, Diversified Biotech). After overnight incubation at 30 °C, 700 r.p.m. and 100% humidity, 30 μl were used to inoculate a deep-well plate containing 1.8 mL LB medium, 25 μg/mL kanamycin per well and plates were sealed with a gas-permeable membrane (Breathe Easier, Diversified Biotech). Cultures were grown at 37 °C and, after they reached an OD_{600} of 0.3, gene expression was induced by adding tetracycline to a final concentration of 2 μg ml^{-1}. Subsequently, the plates were incubated at 20 °C and 240 r.p.m. overnight. Cells were harvested by centrifugation at 4,000 r.p.m. for 20 min at 4 °C, the supernatant discarded and the pellets stored at −20 °C. Lysis was carried out by four freeze–thaw cycles and resuspension of the pellets in 50 mM sodium phosphate, 0.2 mg ml^{-1} lysozyme, 1 mg ml^{-1} polymyxin B, 10 μg ml^{-1} DNAaseI, pH 7.0 and 3 h incubation at room temperature. The lysates were cleared by centrifugation at 4,000 r.p.m. for 20 min at 4 °C.

In a flat bottom ultraviolet–visible microtitre plate (Nunc MicroWell with Nunclon Delta Surface, Thermo Scientific) 150 μl of assay solution that contained 3 mM substrate, 5 U ml^{-1} HRP, 0.15 mg ml^{-1} 4-aminoantipyrine, 1 mM vanillic acid and 2% DMSO in 50 mM sodium phosphate buffer, pH 7.0, was distributed to each well. The reaction was initiated by adding 50 μl of cleared lysate. Activity values were determined by measuring the change of absorption at 498 nm in a microtitre plate reader (Varioskan, Thermo Scientific) and normalizing the slope to the average of three internal wild-type controls was performed in R (version 3.3.2).

Enzyme purification. Purified plasmids of single variants identified in the microtitre plate screen were used to transform BL21 (DE3) pLysS *E. coli* cells (Agilent). Cultures that contained 900 mL of LB medium supplemented with 25 mg ml^{-1} kanamycin and 30 mg ml^{-1} chloramphenicol were inoculated from a starter culture and grown at 37 °C and 240 r.p.m. until they reached OD_{600} of 0.3 and induced by the addition of 0.5 mM IPTG. The enzyme was produced overnight at 25 °C followed by harvesting the cells by centrifugation at 4,500x*g* for

20 min at 4 °C. After discarding the supernatant, the pellets were frozen at −20 °C. The following purification was carried out entirely at 4 °C. Pellets were resuspended in 5 ml of 50 mM sodium phosphate buffer (pH 7.0) that contained 0.2 mg ml^{-1} lysozyme, 1 mg ml^{-1} polymyxin B and 2 mM β-mercaptoethanol and incubated for 3 h. The suspension was subsequently sonicated in the presence of DNase I (NEB). The soluble fraction was recovered by centrifugation at 14,000x*g* for 30 min and CHAO purified by Ni-NTA (Qiagen) affinity chromatography, washing with 10 column volumes of 25 mM imidazole in 50 mM sodium phosphate buffer (pH 7.0), repeated washing with the same amount of 50 mM imidazole 50 mM sodium phosphate buffer pH 7.0) and finally eluting with 250 mM imidazole in 50 mM sodium phosphate buffer (pH 7.0). Samples were analysed by 20% SDS–polyacrylamide gel electrophoresis (GE Healthcare). Fractions that contained CHAO were pooled and dialysed twice against 2 l of 50 mM sodium phosphate (pH 7.0) and 2 mM dithiothreitol, and concentrated using 30 kDa MWCO centrifugation filters (Amicon, Millipore), spinning at 4,000 and 4 °C. The concentration was determined by absorption of FAD at 450 nm using an extinction coefficient[48] of 11,300 M^{-1} cm^{-1} on a NanoDrop 2000 (Thermo Fisher). Typical yields were 10–20 mg l^{-1} culture.

Enzyme kinetics. All the kinetic characterizations were performed with three batches of independently produced enzyme. Purified variants were characterized by monitoring the coupled reaction between hydrogen peroxide, 4-aminoantipyrine and vanillic acid, catalysed by HRP, at 498 nm (ε = 6,234 M^{-1} cm^{-1}) (ref. [19]). The reactions contained 0.23 mg ml^{-1} 4-aminoantipyrine, 1 mM vanillic acid, 5 U HRP and 2% DMSO in 50 mM sodium phosphate buffer (pH 7.0). All the reactions were carried out at 30 °C and were initiated by adding enzyme to a final concentration of either 1 μM or 10 nM for wild-type or PT.1, respectively. For (*R*)-1-phenyl-1,2,3,4-tetrahydroisoquinoline a full Michaelis–Menten kinetic was recorded, whereas for other enzyme–substrate combinations k_{cat}/K_M was determined from a single-point measurement at the lowest substrate concentration at which the reaction could still be observed. Kinetic parameters were determined using Prism 8 (GraphPad Software, Inc.) (Supplementary Fig. 5).

Substrate scope. Substrates **1–8** were characterized with three individually purified enzyme batches by monitoring the coupled reaction between hydrogen peroxide, 4-aminoantipyrine and vanillic acid, catalysed by HRP at 498 nm (ε = 6,234 M^{-1} cm^{-1}) (ref. [19]). The reactions contained 2 mM substrate, 0.23 mg ml^{-1} 4-aminoantipyrine, 1 mM vanillic acid, 5 U HRP and 2% DMSO in 50 mM sodium phosphate buffer (pH 7.0). All the reactions were carried out at 30 °C and were initiated by the addition of the enzyme. The enzyme concentration was varied in the nanomolar to micromolar range to ensure that v_0 was linear for the initial 10% of substrate consumed.

Chiral analysis. Enantiomeric excess was determined via HPLC on a chiral stationary phase using a Waters 717plus Autosampler (Waters Corporation) equipped with two Waters 515 HPLC Pumps (Waters Corporation) and a Waters 996 Photodiode Array Detector (Waters Corporation).

Deracemization of 1-phenyl-1,2,3,4-tetrahydroisoquinoline. The deracemization procedure was adapted from Ghislieri et al.[12]. All deracemizations were carried out with 10 mM 1-phenyl-1,2,3,4-tetrahydroisoquinoline (**7**, 54 mg), 5 μM purified CHAO wild-type or PT.1, 40 mM borane–ammonia complex in 25 ml of 1 M sodium phosphate buffer at pH 7.0, and catalytic amounts of catalase (Sigma Aldrich). The reaction was initiated by adding the oxidase and incubated at 30 °C. Aliquots were periodically removed and analyzed by HPLC. The 250 μl samples were treated with 20 μl of 10 M NaOH and the quenched reaction was extracted with 1 ml of *tert*-butyl methyl ether (TBME). The organic phase was dried over a $MgSO_4$ plug and filtered through a 0.2 μm AcroPrep 96 filter plate (Pall) and separated on a Chiralcel OD-H (Chiral Technologies Europe) column (150 × 4.6 mm, particle diameter = 5 μM) at room temperature, and products were eluted isocratically with 70:30 *n*-hexane:isopropanol at a flow rate of 1 ml min^{-1} (Supplementary Fig. 6d). Once the e.e. converged, the reaction was worked up by adding 200 μl of 10 M NaOH and extracting with 50 ml of TBME. The organic phase was dried over $MgSO_4$ and the solvent removed in vacuo to yield (*S*)-**7** as a white solid (38 mg, 71% yield, 99% e.e.).

High-resolution mass spectrometry (HRMS): calculated [M + H]$^+$ 210.1277, found 210.1275. ^{1}H NMR, 400 MHz, $CDCl_3$ δ ppm: 7.4–7.25 (m, 5H), 7.21–7.14 (m, 2H), 7.10–7.03 (m, 1H), 6.78 (d, *J* = 7.76 Hz, 1H), 5.14 (s, 1H), 3.30 (m, 7.1 Hz, 1H), 3.18–3.01 (m, 2H), 2.92–2.80 (m, 1H), 1.82 (s, 1H). ^{13}C NMR, 100 MHz, $CDCl_3$ δ ppm: 144.7, 138.15, 135.39, 129.0, 128.9, 128.4, 128.1, 127.4, 126.3, 125.7, 62.1, 42.2, 29.7.

Preparative deracemization of compounds 3–6 and 8. The deracemization reactions were set up as whole-cell processes. The respective amine (15 mM) and 60 mM borane–ammonia complex were dissolved in 25 ml of 1 M sodium phosphate buffer at pH 7.0. The reaction was initiated by the addition of 2 g of a wet cell pellet of BL21 (DE3) pLysS *E. coli* cells that expressed PT.1 CHAO. Aliquots were periodically analysed by quenching 250 μl of the reaction mixture with 20 μl of 10 M NaOH, followed by extraction of the amine with 1 ml of TBME. The organic phase was dried over $MgSO_4$ and filtered through a 0.2 μm AcroPrep 96 filter plate (Pall) and analysed by HPLC on a chiral stationary phase. When the e.e. of the product converged, the reaction was quenched by raising the pH to 12 with 10 M NaOH and extracted three times with 25 ml of TBME. The organic phase was combined, dried over $MgSO_4$ and the solvent removed in vacuo.

Compound **3** was analysed on a Chiralcel OD-H (Chiral Technologies Europe) column (150 × 4.6 mm, particle diameter = 5 μM) eluted with a mixture of *n*-hexane and ethanol (95:5) that contained 0.05% diethylamine at 1 ml min^{-1} at room temperature. No enantiomeric enrichment was detected over 48 h. The product was not further purified or analysed.

Deracemization of **4** yielded 19 mg of a colourless oil (35% yield, e.e. 50%). The product enantiomers were separated on a Chiralcel OD-H (Chiral Technologies Europe) column (150 × 4.6 mm, particle diameter = 5 μM) eluted with a mobile phase of *n*-hexane and ethanol (95:5) that contained 0.05% diethylamine at 1 ml min^{-1} at room. The reaction was quenched by raising the pH to 12 with 10 M NaOH when the e.e. converged. After extraction with 3 × 25 ml of TBME, the organic phase was combined, 75 ml of water added and the pH lowered to 1 by the addition of 1 M HCl. The phases were separated and the aqueous phase was again titrated to pH 12 with 10 M NaOH and extracted with 75 ml of TBME, the organic phase was collected, dried over $MgSO_4$ and removed in vacuo and the product analysed again by HPLC on a chiral stationary phase. The retention times were assigned according to the literature[49]. HRMS: calculated [M + H]$^+$ 148.1121, found 148.1122. ^{1}H NMR, 400 MHz, $CDCl_3$ δ ppm: 7.46–7.20 (m, 5H), 3.94 (td, *J* = 7.1, 2.1 Hz, 1H), 1.79–1.65 (m, 2H), 1.42–1.19 (m, 2H), 0.92 (t, *J* = 7.3 Hz, 3H); ^{13}C NMR, 100 MHz, $CDCl_3$ δ ppm: 128.62, 128.50, 127.16, 127.10, 126.46, 126.19, 56.06, 41.20, 19.66, 13.97

Deracemization of **5** yielded 41 mg of yellow oil (75% yield, e.e. 5%). An authentic standard of the racemic compound and the isolated product were separated using a Chiralpak AD-H column (4.6 mm × 250 mm (Daicel)) with a mixture of *n*-hexane and ethanol (98:2), that contained 0.05% diethylamine at 1 ml min^{-1} at room temperature (Supplementary Fig. 6b). The e.e. was determined to be 5% (*S*). The enantiomers were assigned by comparison with literature values of the retention time[35]. HRMS: calculated [M + H]$^+$ 148.1121, found 148.1120. ^{1}H NMR, 400 MHz, $CDCl_3$ δ ppm: 7.34–7.07 (m, 4H), 4.64 (d, *J* = 7.3 Hz, 1H), 3.65–2.97 (m, 4H), 1.87 (d, J = 6.8 Hz, 3H); ^{13}C NMR, 100 MHz, $CDCl_3$ δ ppm: 133.11, 131.15, 129.16, 127.93, 127.32, 126.05, 51.04, 39.12, 25.71, 20.17.

Deracemization of **6** yielded 49 mg of the product as a yellow oil (81% yield, e.e. 98%). The racemic standard and the reaction product were analysed on a Chiralcel OD-H (Chiral Technologies Europe) column (150 × 4.6 mm, particle diameter = 5 μM) at room temperature using *n*-hexane and ethanol (99:1) that contained 0.05% diethylamine as an eluent at a flow rate of 1 ml min^{-1} (Supplementary Fig. 6c). The enantiomers were assigned by comparison to the literature retention times[35]. The e.e. was determined to be 98% (*S*)-**6**. HRMS: calculated [M + H]$^+$ 162.1277, found 162.1281. ^{1}H NMR, 400 MHz, $CDCl_3$ δ ppm: 7.33–7.13 (m, 4H), 4.50 (t, J = 5.6 Hz, 1H), 3.67 (d, J = 11.9 Hz, 1H), 3.42–3.25 (m, 2H), 3.17–3.03 (m, 1H), 2.26–2.17 (m, 2H), 1.24 (t, 3H); ^{13}C NMR, 100 MHz, $CDCl_3$ δ ppm: 131.99, 131.66, 129.21, 127.86, 127.14, 126.40, 56.49, 39.92, 27.37, 25.76, 10.19

Compound **8** was analysed on a Chiralpak AD-H column (4.6 mm × 250 mm (Daicel)) eluted with a mixture of *n*-hexane and ethanol (95:5) that contained 0.05% diethylamine at 1 ml min^{-1} at room temperature. No enantiomeric enrichment was detected over 48 h. The product was not further purified or analysed.

Modelling. The crystal structure of CHAO IH-35A (PDB ID: 4i59) was used as the reference structure for the docking studies. The five mutations in PT.1 (L199V, M226T, Y321S, L353I and P422S) were manually introduced using the ProteinBuilder module in MOE2016.08 (Molecular Operating Environment, Chemical Computing Group). To prepare the structure for docking, the following steps were performed with the MOE2016.08 StructurePreparation module: the structure was protonated at pH 7.4 and structural issues were addressed (adding hydrogens, correct partial charges and hybridization). The resulting structure, as well as all the ligand complexes, were minimized using the AMBER10:EHT (Extended Hückel Theory) force field (termination: root mean square gradient <0.1 kcal mol^{-1} Å^{-2}).

Ligand docking. Potential binding sites were calculated by Site Finder in MOE2016.08. The active site identified next to the co-crystallized ligand was selected as the binding pocket for docking. Docking was executed in MOE2016.08 using the placement method Triangle Matcher and London dG as the scoring method. Of the 1,000 poses returned, 100 were passed to the refinement step. 'Induced Fit' was chosen as the postplacement refinement method with default parameters using GBVI/WSA dG as the final scoring method. Finally, ten poses were finally retained. To confirm the identified poses, the docking was repeated with GOLD 5.5 (CCDC Software) as integrated in MOE2016.08. This re-docking was performed with default parameters (efficiency = 100) using the ChemPLP scoring function and 'Induced Fit' as the refinement method with GBVI/WSA dG as the final scoring function. Of the 100 poses passed to the refinement step, 10 were saved.

Reporting summary. Further information on research design is available in the Nature Research Reporting Summary linked to this article.

Data availability

The data that support the plots and other findings of this study are available from the corresponding author upon reasonable request.

Code availability

No custom code was used to generate data presented in this study.

Received: 1 March 2019; Accepted: 31 July 2019;
Published online: 13 September 2019

References

1. Hönig, M., Sondermann, P., Turner, N. J. & Carreira, E. M. Enantioselective chemo- and biocatalysis: partners in retrosynthesis. *Angew. Chem. Int. Ed.* **56**, 8942–8973 (2017).
2. Constable, D. J. C. et al. Key green chemistry research areas—a perspective from pharmaceutical manufacturers. *Green Chem.* **9**, 411–420 (2007).
3. Mutti, F. G., Knaus, T., Scrutton, N. S., Breuer, M. & Turner, N. J. Conversion of alcohols to enantiopure amines through dual-enzyme hydrogen-borrowing cascades. *Science* **349**, 1525–1529 (2015).
4. Pavlidis, I. V. et al. Identification of (S)-selective transaminases for the asymmetric synthesis of bulky chiral amines. *Nat. Chem.* **8**, 1076–1082 (2016).
5. Aleku, G. A. et al. A reductive aminase from *Aspergillus oryzae*. *Nat. Chem.* **9**, 961–969 (2017).
6. Prier, C. K., Zhang, R. K., Buller, A. R., Brinkmann-Chen, S. & Arnold, F. H. Enantioselective, intermolecular benzylic C–H amination catalysed by an engineered iron-haem enzyme. *Nat. Chem.* **9**, 629–634 (2017).
7. Savile, C.K. et al. Biocatalytic asymmetric synthesis of sitagliptin manufacture. *Science* **329**, 305–309 (2010).
8. Li, T. et al. Efficient, chemoenzymatic process for manufacture of the boceprevir bicyclic [3.1.0]proline intermediate based on amine oxidase-catalyzed desymmetrization. *J. Am. Chem. Soc.* **134**, 6467–6472 (2012).
9. Alexeeva, M., Enright, A., Dawson, M. J., Mahmoudian, M. & Turner, N. J. Deracemization of α-methylbenzylamine using an enzyme obtained by in vitro evolution. *Angew. Chem. Int. Ed.* **41**, 3177–3180 (2002).
10. Yao, P. et al. Biocatalytic route to chiral 2-substituted-1,2,3,4-tetrahydroquinolines using cyclohexylamine oxidase muteins. *ACS Catal.* **8**, 1648–1652 (2018).
11. Ghislieri, D., Houghton, D., Green, A. P., Willies, S. C. & Turner, N. J. Monoamine oxidase (MAO-N) catalyzed deracemization of tetrahydro-β-carbolines: substrate dependent switch in enantioselectivity. *ACS Catal.* **3**, 2869–2872 (2013).
12. Ghislieri, D. et al. Engineering an enantioselective amine oxidase for the synthesis of pharmaceutical building blocks and alkaloid natural products. *J. Am. Chem. Soc.* **135**, 10863–10869 (2013).
13. Agresti, J. J. et al. Ultrahigh-throughput screening in drop-based microfluidics for directed evolution. *Proc. Natl Acad. Sci. USA* **107**, 4004–4009 (2010).
14. Truppo, M. D. Biocatalysis in the pharmaceutical industry: the need for speed. *ACS Med. Chem. Lett.* **8**, 476–480 (2017).
15. Badenhorst, C. P. S. & Bornscheuer, U. T. Getting momentum: from biocatalysis to advanced synthetic biology. *Trends Biochem. Sci.* **43**, 180–198 (2018).
16. Packer, M. S. & Liu, D. R. Methods for the directed evolution of proteins. *Nat. Rev. Genet.* **16**, 379–394 (2015).
17. Bunzel, H. A., Garrabou, X., Pott, M. & Hilvert, D. Speeding up enzyme discovery and engineering with ultrahigh-throughput methods. *Curr. Opin. Struct. Biol.* **48**, 149–156 (2018).
18. Mair, P., Gielen, F. & Hollfelder, F. Exploring sequence space in search of functional enzymes using microfluidic droplets. *Curr. Opin. Chem. Biol.* **37**, 137–144 (2017).
19. Holt, A. & Palcic, M. M. A peroxidase-coupled continuous absorbance plate-reader assay for flavin monoamine oxidases, copper-containing amine oxidases and related enzymes. *Nat. Protocols* **1**, 2498–2505 (2006).
20. Sadler, J. C., Currin, A. & Kell, D. B. Ultra-high throughput functional enrichment of large monoamine oxidase (MAO-N) libraries by fluorescence activated cell sorting. *Analyst* **143**, 4747–4755 (2018).
21. Clausell-Tormos, J. et al. Droplet-based microfluidic platforms for the encapsulation and screening of mammalian cells and multicellular organisms. *Chem. Biol.* **15**, 427–437 (2008).
22. Dressler, O. J., Casadevall i Solvas, X. & DeMello, A. J. Chemical and biological dynamics using droplet-based microfluidics. *Annu. Rev. Anal. Chem.* **10**, 1–24 (2017).
23. Baret, J.-C. et al. Fluorescence-activated droplet sorting (FADS): efficient microfluidic cell sorting based on enzymatic activity. *Lab Chip* **9**, 1850–1858 (2009).
24. Beneyton, T. et al. High-throughput screening of filamentous fungi using nanoliter-range droplet-based microfluidics. *Sci. Rep.* **6**, 27223 (2016).
25. Beneyton, T. et al. Droplet-based microfluidic high-throughput screening of heterologous enzymes secreted by the yeast *Yarrowia lipolytica*. *Microb. Cell Fact.* **16**, 18 (2017).
26. Kintses, B. et al. Picoliter cell lysate assays in microfluidic droplet compartments for directed enzyme evolution. *Chem. Biol.* **19**, 1001–1009 (2012).
27. Li, G. et al. New recombinant cyclohexylamine oxidase variants for deracemization of secondary amines by orthogonally assaying designed mutants with structurally diverse substrates. *Sci. Rep.* **6**, 24973 (2016).
28. Li, G. et al. Substrate profiling of cyclohexylamine oxidase and its mutants reveals new biocatalytic potential in deracemization of racemic amines. *Appl. Microbiol. Biotechnol.* **98**, 1681–1689 (2014).
29. Obexer, R. et al. Emergence of a catalytic tetrad during evolution of a highly active artificial aldolase. *Nat. Chem.* **9**, 50–56 (2017).
30. Colin, P. Y. et al. Ultrahigh-throughput discovery of promiscuous enzymes by picodroplet functional metagenomics. *Nat. Commun.* **6**, 10008 (2015).
31. Ma, F. et al. Efficient molecular evolution to generate enantioselective enzymes using a dual-channel microfluidic droplet screening platform. *Nat. Commun.* **9**, 1030 (2018).
32. Najah, M. et al. Droplet-based microfluidics platform for ultra-high-throughput bioprospecting of cellulolytic microorganisms. *Chem. Biol.* **21**, 1722–1732 (2014).
33. Gielen, F. et al. Ultrahigh-throughput-directed enzyme evolution by absorbance-activated droplet sorting (AADS). *Proc. Natl Acad. Sci. USA* **113**, E7383–E7389 (2016).
34. Wang, X. et al. Raman-activated droplet sorting (RADS) for label-free high-throughput screening of microalgal single-cells. *Anal. Chem.* **89**, 12569–12577 (2017).
35. Li, G. et al. Simultaneous engineering of an enzyme's entrance tunnel and active site: the case of monoamine oxidase MAO-N. *Chem. Sci.* **8**, 4093–4099 (2017).
36. Pickl, M. et al. Kinetic resolution of sec-thiols by enantioselective oxidation with rationally engineered 5-(hydroxymethyl)furfural oxidase. *Angew. Chem. Int. Ed.* **57**, 2864–2868 (2018).
37. Escalettes, F. & Turner, N. J. Directed evolution of galactose oxidase: generation of enantioselective secondary alcohol oxidases. *ChemBioChem* **9**, 857–860 (2008).
38. Azuma, Y., Zschoche, R., Tinzl, M. & Hilvert, D. Quantitative packaging of active enzymes into a protein cage. *Angew. Chem. Int. Ed.* **55**, 1531–1534 (2016).
39. Roderer, K. et al. Functional mapping of protein–protein interactions in an enzyme complex by directed evolution. *PLoS ONE* **9**, e116234 (2014).
40. Horton, R. M., Hunt, H. D., Ho, S. N., Pullen, J. K. & Pease, L. R. Engineering hybrid genes without the use of restriction enzymes: gene splicing by overlap extension. *Gene* **77**, 61–68 (1989).
41. Obexer, R., Pott, M., Zeymer, C., Griffiths, A. D. & Hilvert, D. Efficient laboratory evolution of computationally designed enzymes with low starting activities using fluorescence-activated droplet sorting. *Protein Eng. Des. Sel.* **29**, 355–366 (2016).
42. Frenz, L., Blank, K., Brouzes, E. & Griffiths, A. D. Reliable microfluidic on-chip incubation of droplets in delay-lines. *Lab Chip* **9**, 1344–1348 (2009).
43. Siegel, A. C., Bruzewicz, D. A., Weibel, D. B. & Whitesides, G. M. Microsolidics: fabrication of three-dimensional metallic microstructures in poly(dimethylsiloxane). *Adv. Mater.* **19**, 727–733 (2007).
44. Panke, S., Meyer, A., Huber, C. M., Witholt, B. & Wubbolts, M. G. An alkane-responsive expression system for the production of fine chemicals. *Appl. Environviron. Microbiol.* **65**, 2324–2332 (1999).
45. Anna, S. L., Bontoux, N. & Stone, H. A. Formation of dispersions using 'flow focusing' in microchannels. *Appl. Phys. Lett.* **82**, 364–366 (2003).
46. Abate, A. R. et al. Impact of inlet channel geometry on microfluidic drop formation. *Phys. Rev. E* **80**, 026310 (2009).
47. Bosley, A. D. & Ostermeier, M. Mathematical expressions useful in the construction, description and evaluation of protein libraries. *Biomol. Eng.* **22**, 57–61 (2005).
48. Lewis, J. A. & Escalante-Semerena, J. C. The FAD-dependent tricarballylate dehydrogenase (TcuA) enzyme of *Salmonella enterica* converts tricarballylate into *cis*-aconitate. *J. Bacteriol.* **188**, 5479–5486 (2006).
49. Peng, Y. et al. Engineering chiral porous metal–organic frameworks for enantioselective adsorption and separation. *Nat. Commun.* **5**, 4406 (2014).

Acknowledgements

This work was generously supported by the Swiss National Science Foundation and the ETH Zurich.

Author contributions

A.P.G. and R.O. initiated the project; A.D. and M.P. performed the experiments and analysed the data; L.F. performed the molecular modelling; A.D., A.D.G. and D.H. co-wrote the paper.

Competing interest

The authors declare no competing interests.

Additional information

Supplementary information is available for this paper at https://doi.org/10.1038/s41929-019-0340-5.

Reprints and permissions information is available at www.nature.com/reprints.

Correspondence and requests for materials should be addressed to D.H.

nature research

Corresponding author(s): Donald Hilvert

Last updated by author(s): Jul 5, 2019

Reporting Summary

Nature Research wishes to improve the reproducibility of the work that we publish. This form provides structure for consistency and transparency in reporting. For further information on Nature Research policies, see Authors & Referees and the Editorial Policy Checklist.

Statistics

For all statistical analyses, confirm that the following items are present in the figure legend, table legend, main text, or Methods section.

n/a	Confirmed	
☐	☒	The exact sample size (*n*) for each experimental group/condition, given as a discrete number and unit of measurement
☐	☒	A statement on whether measurements were taken from distinct samples or whether the same sample was measured repeatedly
☒	☐	The statistical test(s) used AND whether they are one- or two-sided *Only common tests should be described solely by name; describe more complex techniques in the Methods section.*
☒	☐	A description of all covariates tested
☒	☐	A description of any assumptions or corrections, such as tests of normality and adjustment for multiple comparisons
☐	☒	A full description of the statistical parameters including central tendency (e.g. means) or other basic estimates (e.g. regression coefficient) AND variation (e.g. standard deviation) or associated estimates of uncertainty (e.g. confidence intervals)
☒	☐	For null hypothesis testing, the test statistic (e.g. *F*, *t*, *r*) with confidence intervals, effect sizes, degrees of freedom and *P* value noted *Give P values as exact values whenever suitable.*
☒	☐	For Bayesian analysis, information on the choice of priors and Markov chain Monte Carlo settings
☒	☐	For hierarchical and complex designs, identification of the appropriate level for tests and full reporting of outcomes
☒	☐	Estimates of effect sizes (e.g. Cohen's *d*, Pearson's *r*), indicating how they were calculated

Our web collection on statistics for biologists contains articles on many of the points above.

Software and code

Policy information about availability of computer code

Data collection	No custom software was used for the collecting the data within this study
Data analysis	CLC Genomics Workbench 7 was used for sequence alignment R version 3.3.2 and Prism 8 (GraphPad Software, Inc.) was used for the analysis and visualization of the enzyme characterization MOE2016.08 (Molecular Operating Environment, Chemical Computing Group) and GOLD 5.5 (CCDC Software) was used for molecular modeling

For manuscripts utilizing custom algorithms or software that are central to the research but not yet described in published literature, software must be made available to editors/reviewers. We strongly encourage code deposition in a community repository (e.g. GitHub). See the Nature Research guidelines for submitting code & software for further information.

Data

Policy information about availability of data

All manuscripts must include a data availability statement. This statement should provide the following information, where applicable:

- Accession codes, unique identifiers, or web links for publicly available datasets
- A list of figures that have associated raw data
- A description of any restrictions on data availability

The authors declare that all data supporting the results from this study are made available within this paper and the respective supplementary information.

Field-specific reporting

Please select the one below that is the best fit for your research. If you are not sure, read the appropriate sections before making your selection.

☒ Life sciences ☐ Behavioural & social sciences ☐ Ecological, evolutionary & environmental sciences

For a reference copy of the document with all sections, see nature.com/documents/nr-reporting-summary-flat.pdf

Life sciences study design

All studies must disclose on these points even when the disclosure is negative.

Sample size	Enzyme characterization was carried out in triplicate. Individual batches were purified separately.
Data exclusions	No data were excluded from the manuscript
Replication	All methods used are carefully described in the online methods section and are reproducible by an expert of the field
Randomization	Not applicable
Blinding	Blinding was not relevant for the experiments carried out in this study

Reporting for specific materials, systems and methods

We require information from authors about some types of materials, experimental systems and methods used in many studies. Here, indicate whether each material, system or method listed is relevant to your study. If you are not sure if a list item applies to your research, read the appropriate section before selecting a response.

Materials & experimental systems

n/a	Involved in the study
☒	☐ Antibodies
☒	☐ Eukaryotic cell lines
☒	☐ Palaeontology
☒	☐ Animals and other organisms
☒	☐ Human research participants
☒	☐ Clinical data

Methods

n/a	Involved in the study
☒	☐ ChIP-seq
☒	☐ Flow cytometry
☒	☐ MRI-based neuroimaging